Functional Materials 21, No.2 (2014)

Structural behaviour of continuous solid solution $SmCo_{1-x}Fe_xO_3$

O.V.Kharko, L.O.Vasylechko, S.B.Ubizskii, A.Pashuk, Yu.Prots*

Lviv Polytechnic National University, 12 Bandera Str.,
79013 Lviv, Ukraine
*Max-Planck-Institut fur Chemische Physik fester Stoffe,
40 Nothnitzer Str., 01187 Dresden, Germany

Received November 14, 2013

Phase and structural behaviour in the $SmCoO_3$–$SmFeO_3$ pseudobinary system has been investigated at the ambient conditions in a whole concentration range by means of X-ray powder diffraction technique applied laboratory and synchrotron radiation sources. Series of mixed samarium cobaltites-ferrites $SmCo_{1-x}Fe_xO_3$ was obtained by the solid state reaction in air at 1573 K. Formation of a continuous solid solution $SmCo_{1-x}Fe_xO_3$ with orthorhombic perovskite structure ($GdFeO_3$ type, space group *Pbnm*) has been revealed. Crystal structure parameters of the mixed samarium cobaltites-ferrites, as well as nominally pure $SmCoO_3$ and $SmFeO_3$ have been established by full profile Rietveld refinement. Based on the analysis of structural parameters, an influence of the cation substitution on the deformation of the orthorhombic perovskite structure in the $SmCo_{1-x}Fe_xO_3$ series has been established.

Методом порошковой дифракции рентгеновского и синхротронного излучения исследованы фазовые и структурные соотношения в псевдо-бинарной системе $SmCoO_3$–$SmFeO_3$ при комнатной температуре в полном концентрационном интервале. Серия смешанных кобальтитов-хромитов $SmCo_{1-x}Fe_xO_3$ получена методом твердофазного синтеза на воздухе при температуре 1573 К. Установлено образование непрерывного твердого раствора $SmCo_{1-x}Fe_xO_3$ с ромбической структурой перовскита типа $GdFeO_3$ (пространственная группа *Pbnm*). Используя полнопрофильный метод Ритвельда, уточнены структурные параметры новых смешанных кобальтитов-хромитов $SmCo_{1-x}Fe_xO_3$, а также номинально чистых соединений $SmCoO_3$ и $SmFeO_3$. На основе анализа структурных параметров установлено влияние катионного замещения на степень деформаций ромбической перовскитной структуры в ряду $SmCo_{1-x}Fe_xO_3$.

Структурна поведінка неперервного твердого розчину $SmCo_{1-x}Fe_xO_3$. *О.В.Харко, Л.О.Василечко, С.Б.Убізський, А.В.Пашук, Ю.Проць.*

Методом порошкової дифракції рентгенівського та синхротронного випромінювання досліджено фазову та структурну поведінку в системі $SmCoO_3$–$SmFeO_3$ при кімнатній температурі у повному концентраційному інтервалі. Серію змішаних кобальтитів-феритів самарію $SmCo_{1-x}Fe_xO_3$ одержано твердофазним синтезом на повітрі при 1573 К. Встановлено утворення неперервного твердого розчину $SmCo_{1-x}Fe_xO_3$ із ромбічною структурою перовскиту типу $GdFeO_3$ (просторова група *Pbnm*). Використовуючи повнопрофільний метод Рітвельда, уточнено параметри кристалічної структури змішаних кобальтитів-феритів самарію $SmCo_{1-x}Fe_xO_3$, а також номінально чистих сполук $SmCoO_3$ і $SmFeO_3$. На основі аналізу структурних даних встановлено вплив катіонного заміщення на ступінь деформації перовскитної структури у низці $SmCo_{1-x}Fe_xO_3$.

1. Introduction

Complex oxides with perovskite structure RMO_3, where R and M are rare earth and transition metals, respectively, represent an important class of functional materials. In particular, the $RCoO_3$ and $RFeO_3$ compounds are used in thermoelectric devices, solid oxide fuel cells [1–3], as membranes for partial oxidation of methane and cleaning oxygen, as catalysts for CO oxidation and decomposition of NO_x, as sensory materials [4–6]. Complementary, the interest in the rare earth cobaltites $RCoO_3$ is also stimulated by their unique fundamental physical properties, such as temperature induced metal-insulator transitions and different types of magnetic ordering, which are strongly dependent on the spin state of Co^{3+} cations. The latter undergo a thermally driven transition from a low-spin (LS) to intermediate-spin (IS) and high-spin (HS) states. Stabilization and purposeful tuning of the different spin states of Co^{3+} can be achieved by a mutual substitution of cations and they can be controlled by probing of thermal expansion, which is very sensitive to spin-state transitions and crystal-field excitations as well as their coupling to the lattice [7–14].

Among of $RCoO_3$–$RFeO_3$ systems, the most studies are devoted to the systems with La [15–20] and Pr [21–23]. In the $LaCoO_3$–$LaFeO_3$ system, two kinds of solid solutions $LaCo_{1-x}Fe_xO_3$ with rhombohedral and orthorhombic perovskite structure are formed at $x \le 0.5$ and $x \ge 0.4$, respectively [15]. Temperature-induced structural transitions from the rhombohedral phase into the orthorhombic one are detected in $LaCo_{0.5}Fe_{0.5}O_3$ and $LaCo_{0.42}Fe_{0.58}O_3$ samples in [16]. Magnetic properties of $LaCo_{1-x}Fe_xO_3$ were explained assuming a low spin state of the Co^{3+} ions, whereas antiferromagnetism is caused by magnetic interactions between the Fe^{3+} ions. Based on the results obtained the combined crystal and magnetic phase diagram of the $LaCo_{1-x}Fe_xO_3$ system has been constructed [16].

Phase and structural behaviour in the $PrCoO_3$–$PrFeO_3$ system has been studied in the temperature range of 298–1173 K by means of *in situ* high-resolution X-ray synchrotron powder diffraction [21–23]. Formation of continuous solid solution with orthorhombic perovskite structure has been revealed in this system. Peculiarity of the $PrCo_{1-x}Fe_xO_3$ solid solution is the lattice parameter crossover which results in four regions of solid solutions with different relations of the unit cell dimensions [21, 22]. All $PrCo_{1-x}Fe_xO_3$ samples show anomalies in thermal expansion, which are evidently associated with partial transitions of Co^{3+} ions to the higher spin states. The influence of cation substitution on the structural and thermal parameters of the $PrCoO_3$–$PrFeO_3$ system has been established [23].

All other $RCoO_3$–$RFeO_3$ systems are much less studied. In [24] low-temperature specific heat measurements have been carried out on the $NdCo_{1-x}Fe_xO_3$ perovskite system ($x = 0$, 0.1, 0.5, 0.75, 1). Electrical and sensory properties of the nanocrystalline neodymium cobaltites-ferrites were studied in [25]. It was showed that the $NdCo_{1-x}Fe_xO_3$ samples with $x = 0.5$–1 adopt an orthorhombic structure and both the unit cell volume and grain size decrease with an increasing of the Co content.

Nanocrystalline $SmCo_{1-x}Fe_xO_3$ powders with perovskite structure were prepared by sol-gel method at 1073 K [26]. It was found that conductivity of the materials increases with the temperature rising and achieve the maximum at 1073 K for the sample with $x = 0.8$. The study of O_3 and NO_2 sensing properties of the fine particles of the $SmCo_{1-x}Fe_xO_3$ perovskite oxides was performed in [27]. Compared with $SmFeO_3$, the Co-contained oxides show good response and recovery behaviour even at low temperatures and can be candidates for a low temperature sensing material. The influence of the Co content on microstructure, electrical and ethanol-sensing properties of $SmCo_{1-x}Fe_xO_3$ perovskites was investigated in [28]. It was shown that the lattice constant, unit cell volume and average grain size decrease with an increase in the Co content due to forming oxygen vacancies in $SmCo_{1-x}Fe_xO_3$.

However, the information about the structural parameters of the mixed $RCo_{1-x}Fe_xO_3$ perovskites with rare earth heavier as Pr is very limited. Only the lattice parameters for the selected $NdCo_{1-x}Fe_xO_3$ and $SmCo_{1-x}Fe_xO_3$ specimens, which are rather disputable, are reported in [25] and [28].

The aim of the present work is the detailed phase and structural investigations of the mixed cobaltites-ferrites formed in the $SmCoO_3$–$SmFeO_3$ pseudo-binary systems. Preliminary results on the crystal structure and anomalous lattice expansion in the $RCo_{1-x}Fe_xO_3$ systems with Pr, Nd, Sm and Eu have been represented at the conference [29].

2. Experimental

Series of mixed samarium cobaltites-ferrites of nominal composition $SmCo_{1-x}Fe_xO_3$ (x = 0.1, 0.3, 0.5, 0.7 and 0.9), as well as end members of this system $SmCoO_3$ and $SmFeO_3$ were obtained by solid-state reaction technique from constituent oxides Sm_2O_3, Co_3O_4 and Fe_2O_3. Stoichiometric amount of the oxide powders (about 1.3–1.5 g) were ball-milled in the ethanol for 4 h with 400 rpm. After drying of the slurry, the mixtures were loaded in alumina boats, heated in air up to 1573 K for 6 h, reacted at this temperature for 24 h and slowly cooled down to 373 K within next 12 h. X-ray phase and structural characterisation of the $SmCo_{1-x}Fe_xO_3$ samples at room temperature was performed by using Huber imaging plate Guinier camera G670 ($CuK_{\alpha 1}$ radiation, λ = 1.54056 Å). Crystal structures of the end members of the system — $SmCoO_3$ and $SmFeO_3$ compounds — have been studied by means of high-resolution X-ray powder diffraction applied synchrotron radiation. Corresponding experiments were performed at the beamline B2 of HASYLAB/DESY (Hamburg, Germany). The diffraction experiments were carried out in Debye-Scherrer capillary vertical geometry at the powder diffractometer equipped with on-site readable imaging plate detector OBI [30, 31]. The diffraction patterns were collected in the 2θ range 3–65 degrees with a step size of 0.004 deg. The wavelength of 0.53842 Å was selected using a Si(111) double flat-crystal monochromator and determined from eight reflection positions of LaB_6 reference material (NIST SRM 660a). All crystallographic calculations including refinements of the lattice parameters, fractional coordinates of the atoms and their displacement parameters were performed by full-profile Rietveld technique implemented in the program package WinCSD [32].

3. Results and discussion

X-ray powder diffraction examination revealed that all samples synthesized possess orthorhombic perovskite structure isotypic with $GdFeO_3$. No extra phases were detected in the specimens within a sensitivity limits of the method 2–3 wt. %. Full profile Rietveld refinement, performed in space group *Pbnm*, led to a good agreement between calculated and experimental patterns and confirms isostructurality of the mixed cobaltites-ferrites $SmCo_{1-x}Fe_xO_3$ with the end-members of the system — $SmCoO_3$ and $SmFeO_3$. As an example, Fig. 1 demonstrates the fragments of diffraction patterns of $SmCo_{0.3}Fe_{0.7}O_3$ and $SmCo_{0.7}Fe_{0.3}O_3$ specimens, in comparison with the corresponding calculated patterns. Refined values of lattice parameters, positional and displacement parameters of the atoms in the structures investigated, as well as the corresponding residuals, are collected in Table 1. Selected interatomic distances, calculated from the structural parameters obtained, are presented in Table 2.

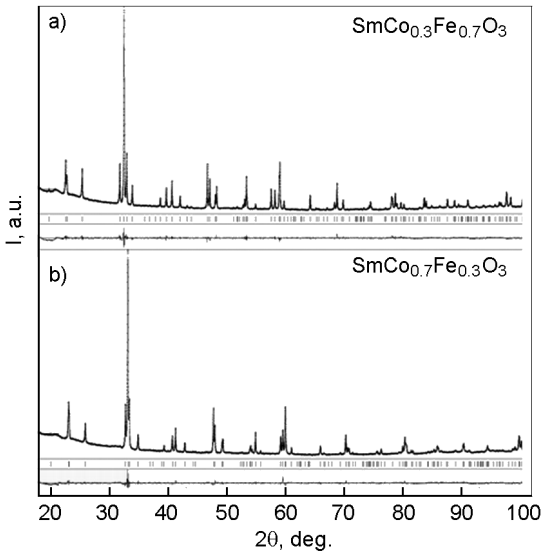

Fig. 1. Laboratory X-ray powder diffraction patterns (small circles) of $SmCo_{0.3}Fe_{0.7}O_3$ (top) and $SmCo_{0.7}Fe_{0.3}O_3$ (bottom) in comparison with the calculated patterns. The difference between measured and calculated profiles is shown as a curve below the diagrams, reflection positions are indicated by ticks.

Crystal structure of the mixed cobaltites-ferrites $SmCo_{1-x}Fe_xO_3$ can be described as a framework of corner-sharing MO_6 (M = Co/Fe) octahedra with the Sm atoms occupying hollow spaces between them (Fig. 2). But in contrast to the ideal cubic perovskite structure, mutual displacements of the rare earth and oxygen atoms from their ideal positions are observed in the orthorhombic *Pbnm* structure (Table 1). Such displacements of rare earth and oxygen atoms lead to a significant redistribution of interatomic distances in $SmCo_{1-x}Fe_xO_3$. In particular, instead of 12 equal Sm–O distances in the cubic perovskite structure, there is a set of twelve Sm–O distances (typically grouped in 1-2-1-2-2-1-1-2), which are distributed in a rather broad range from 2.24 to 3.44 Å (Table 2). The six Co/Fe–O bonds, which are equal in the cubic structure, split

Table 1. Lattice parameters, coordinates and displacement parameters of atoms in $SmCo_{1-x}Fe_xO_3$ structures

Atoms, sites	Parameters	x in $SmCo_{1-x}Fe_xO_3$						
		0	0.1	0.3	0.5	0.7	0.9	1
	a, Å	5.2876(2)	5.29830(9)	5.32201(7)	5.34459(6)	5.36493(6)	5.38959(6)	5.39827(8)
	b, Å	5.3502(1)	5.37120(9)	5.42189(7)	5.47472(6)	5.52267(7)	5.57932(6)	5.59872(8)
	c, Å	7.5007(2)	7.5200(1)	7.56172(10)	7.60379(8)	7.64282(9)	7.69010(8)	7.7071(1)
Sm, 4c	x	−0.0078(3)	−0.0090(3)	−0.0092(3)	−0.0113(3)	−0.0102(3)	−0.0121(3)	−0.0117(2)
	y	0.0465(2)	0.0483(2)	0.0501(2)	0.0528(2)	0.0541(2)	0.0558(2)	0.0564(2)
	z	1/4	1/4	1/4	1/4	1/4	1/4	1/4
	B_{iso}, Å^2	0.77(1)	0.98(2)	0.61(2)	0.49(2)	0.47(2)	0.41(2)	0.77(1)
Fe/Co*, 4b	x	0	1/2	0	0	0	0	0
	y	1/2	1/2	1/2	1/2	1/2	1/2	1/2
	z	0	0	0	0	0	0	0
	B_{iso}, Å^2	0.60(3)	1.36(4)	0.98(4)	1.06(4)	0.59(5)	0.40(4)	0.60(4)
O1, 4c	x	0.080(3)	0.097(2)	0.082(2)	0.1032(15)	0.091(2)	0.087(2)	0.096(2)
	y	0.494(2)	0.486(2)	0.4780(15)	0.4717(15)	0.4759(15)	0.4820(14)	0.481(2)
	z	1/4	1/4	1/4	1/4	1/4	1/4	1/4
	B_{iso}, Å^2	1.2(3)	2.0(3)	1.3(3)	1.0(3)	1.2(3)	2.1(3)	0.1(2)
O2, 8d	x	−0.289(2)	−0.2929(15)	−0.2901(14)	−0.2937(13)	−0.3019(12)	−0.3013(12)	−0.3011(14)
	y	0.288(2)	0.2934(15)	0.2805(14)	0.2912(12)	0.2855(13)	0.2993(12)	0.3004(14)
	z	0.040(2)	0.0220(13)	0.0527(9)	0.0485(8)	0.0422(9)	0.0428(9)	0.0489(10)
	B_{iso}, Å^2	0.8(2)	1.1(2)	1.6(2)	1.00(15)	0.7(2)	1.5(2)	0.56(15)
R_I		0.0928	0.0866	0.0938	0.0704	0.0796	0.0741	0.0987
R_P		0.1546	0.1168	0.1159	0.1172	0.1175	0.1220	0.1767

* The occupancies of the Fe/Co position were fixed at nominal composition, due to the small difference of the scattering factors of Co and Fe.

into two shorter, two medium, and two longer ones (Table 2). Due to the deformation of the cation sublattice, a redistribution of Sm–Sm, Sm–Co/Fe, and Co/Fe–Co/Fe distances is also observed (Table 2). Mutual displacement of oxygen atoms in the $SmCo_{1-x}Fe_xO_3$ structures results in the considerable deviation of M–O–M (M = Co/Fe) angles from 180° (Table 2) and it is reflected by cooperative tilts of the MO_6 octahedra, as it is shown in Fig. 2.

An analysis of the concentration dependence of the lattice parameters and unit cell volume of the $SmCo_{1-x}Fe_xO_3$ (Fig. 3) proves the formation of a continuous solid solution in the $SmCoO_3$–$SmFeO_3$ system. All lattice parameters increase practically linearly with the increasing of Fe content in $SmCo_{1-x}Fe_xO_3$ in accordance with Vegard's rule. In contrast to the $PrCoO_3$–$PrFeO_3$ sys-

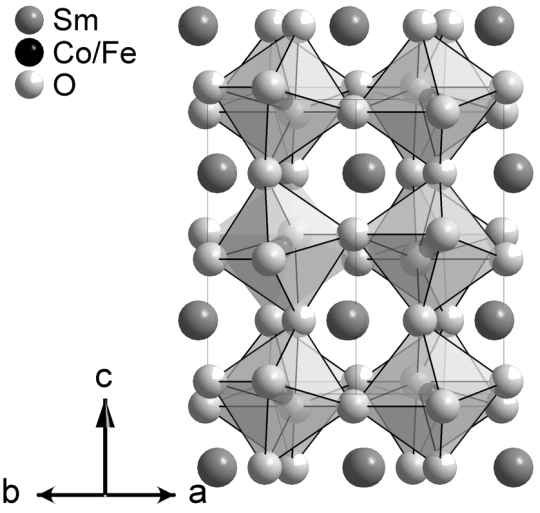

Fig. 2. Orthorhombic $SmCo_{1-x}Fe_xO_3$ structure as a framework of corner-shared octahedra.

Table 2. Selected interatomic distances (Å) and angles (degs.) in $SmCo_{1-x}Fe_xO_3$ structures

Atoms*		x in $SmCo_{1-x}Fe_xO_3$						
		0	0.1	0.3	0.5	0.7	0.9	1
M	–2O2	1.923(10)	1.914(8)	1.928(8)	1.973(7)	1.929(7)	2.000(7)	2.006(8)
	–2O1	1.931(3)	1.933(3)	1.944(2)	1.985(2)	1.976(2)	1.981(2)	1.997(3)
	–2O2	1.932(10)	1.977(8)	1.990(8)	1.977(7)	2.032(7)	2.011(7)	2.030(8)
Sm	–1O1	2.245(14)	2.289(11)	2.306(9)	2.226(8)	2.292(9)	2.330(9)	2.286(10)
	–2O2	2.348(10)	2.326(9)	2.346(7)	2.342(7)	2.396(7)	2.366(7)	2.346(8)
	–1O1	2.438(11)	2.358(9)	2.371(8)	2.374(8)	2.391(8)	2.436(8)	2.448(9)
	–2O2	2.555(10)	2.447(9)	2.454(7)	2.515(7)	2.570(7)	2.610(7)	2.595(8)
	–2O2	2.588(10)	2.714(9)	2.728(7)	2.690(6)	2.650(7)	2.648(7)	2.684(8)
	–1O1	3.005(11)	3.064(11)	3.075(9)	3.195(8)	3.143(9)	3.123(9)	3.179(10)
	–1O1	3.074(14)	3.099(9)	3.140(8)	3.240(8)	3.239(8)	3.246(8)	3.272(9)
	–2O2	3.232(10)	3.286(9)	3.315(7)	3.370(7)	3.363(7)	3.442(7)	3.1437(7)
O2	–2O2	2.714(14)	2.719(11)	2.744(11)	2.777(10)	2.787(9)	2.828(9)	2.853(11)
	–1O1	2.682(13)	2.685(12)	2.702(10)	2.744(8)	2.721(8)	2.810(8)	2.827(10)
	–1O1	2.713(12)	2.689(12)	2.708(10)	2.797(9)	2.830(9)	2.810(8)	2.841(10)
	–1O1	2.737(14)	2.752(10)	2.769(8)	2.806(8)	2.801(10)	2.820(10)	2.834(11)
	–1O1	2.780(15)	2.843(11)	2.860(9)	2.853(9)	2.839(10)	2.835(10)	2.854(11)
	–2O2	2.739(14)	2.785(11)	2.797(11)	2.809(9)	2.817(10)	2.844(10)	2.854(11)
Sm	–2M*	3.0667(7)	3.0705(6)	3.0866(6)	3.1002(6)	3.1173(6)	3.1371(6)	3.1437(7)
	–2M	3.218(1)	3.224(2)	3.236(1)	3.243(1)	3.263(1)	3.272(1)	3.280(1)
	–2M	3.284(1)	3.294(2)	3.315(1)	3.341(1)	3.351(1)	3.378(1)	3.382(1)
	–2M	3.4737(7)	3.4935(7)	3.5314(6)	3.5745(7)	3.6082(7)	3.6494(7)	3.6633(8)
Sm	–2Sm	3.705(2)	3.712(2)	3.731(2)	3.742(2)	3.775(2)	3.789(2)	3.802(2)
	–2Sm	3.7840(2)	3.7964(2)	3.8209(2)	3.8475(2)	3.8694(2)	3.8974(2)	3.9068(3)
	–2Sm	3.818(2)	3.833(2)	3.868(2)	3.911(2)	3.926(2)	3.971(2)	3.977(2)
M	–2M	3.7503(1)	3.7601(1)	3.7809(1)	3.8019(1)	3.8214(1)	3.8450(1)	3.8533(1)
	–4M	3.7610(1)	3.7724(1)	3.7987(1)	3.8255(1)	3.8497(1)	3.8787(1)	3.8885(1)
	M–O1–M	152.49(6)	153.06(5)	153.01(4)	146.45(4)	150.47(4)	152.10(4)	149.47(4)
	M–O2–M	154.58(6)	151.55(5)	151.60(4)	151.18(4)	152.75(4)	150.53(4)	148.96(4)

* $M = Co_{1-x}Fe_x$

tem recently investigated [21–23], the lattice parameter crossover is not observed in the $SmCoO_3$–$SmFeO_3$ system, because $SmCoO_3$ and $SmFeO_3$ adopt the same sequence of the unit cell parameters ($b_p > cp > a_p$) within the orthorhombic $GdFeO_3$ type of structure.

The analysis of the concentration dependence of interatomic distances shows increase of the degree of deformation of the orthorhombic perovskite structure in $SmCo_{1-x}Fe_xO_3$ series, which is particularly reflected in a divergence behaviour of Sm–Co/Fe and Sm–Sm interatomic distances with increasing of Fe content (Table 2). As it was shown in [33] and [34], an analysis of the ratio of cation-cation distances $(AB)_{max}/(AB)_{min}$ and $(AA)_6/(BB)_6$ in the ABO_3 perovskites is very useful tool for the characterisation of the deformation of the perovskites structures. In the ideal cubic perovskite structure, all individual A–B, A–A, and B–B distances are equal and hence it is trivial that the ratios of $(AB)_{max}/(AB)_{min}$ and $(AA)_6/(BB)_6$ are equal to unity. Concentration dependency of the average distance ratio $(SmSm)_6/(MM)_6$ and $(SmM)_{max}/(SmM)_{min}$ (Fig. 4, top) indicates the increase of the orthorhombic deformation in $SmCo_{1-x}Fe_xO_3$ series with the

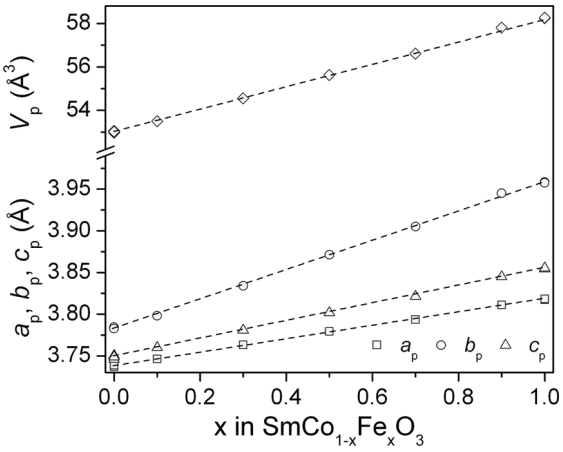

Fig. 3. Concentration dependences of normalized lattice parameters and unit cell volumes in $SmCo_{1-x}Fe_xO_3$ series. Lattice parameters and cell volumes of the orthorhombic cell are normalized to the perovskite one as follows: $a_p = a_o/\sqrt{2}$, $b_p = b_o/\sqrt{2}$, $c_p = c_o/2$, $V_p = V_o/4$.

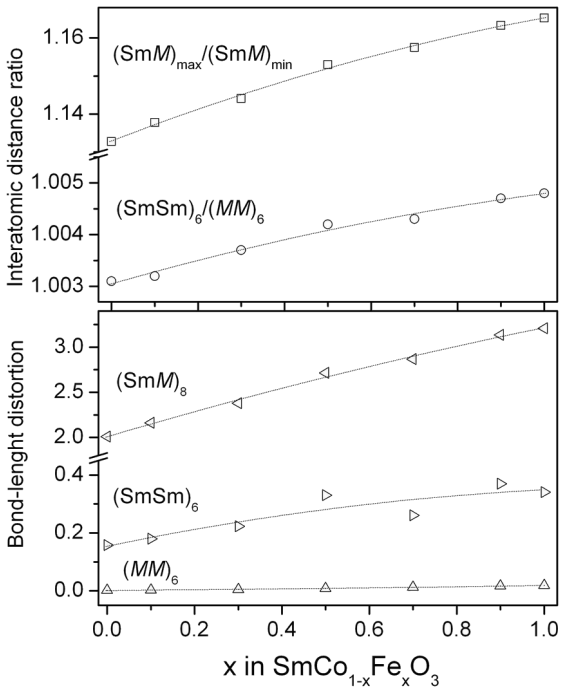

Fig. 4. The ratios of interatomic distances $(SmM)_{max}/(SmM)_{min}$ and $(SmSm)_6/(MM)_6$ ($M = Co_{1-x}Fe_x$) and bond-length distortion of the polyhedra (Δ) in $SmCo_{1-x}Fe_xO_3$ solid solutions as a function of Fe concentration. $\Delta = (1/n)\sum(r_i - r)/r^2 \cdot 10^3$, where r_i and r are the individual and average values of the interatomic distances in the polyhedra with coordination number n [35]. Experimental data points were fitted by second-order polynomials.

increasing x values. Increasing deformations of the perovskite structure in the $SmCoO_3$–$SmFeO_3$ series is also illustrated by the concentration dependences of the bond-length distortion of the polyhedra (Δ), calculated after [35, 36] for the closest Sm–Sm and Sm–M contacts (Fig. 4, bottom).

4. Conclusions

Single-phase samples of the mixed samarium cobaltites-ferrites $SmCo_{1-x}Fe_xO_3$ (x = 0.1, 0.3, 0.5, 0.7 and 0.9) as well as nominally pure $SmCoO_3$ and $SmFeO_3$ were successfully prepared by solid-state reaction in air at 1573 K. Formation of continuous solid solution $SmCo_{1-x}Fe_xO_3$ with orthorhombic perovskite structure has been revealed by means of powder diffraction technique applying both laboratory X-ray and synchrotron radiation sources. Analysis of structural parameters, obtained by full profile Rietveld refinement routine, show that increase of the iron content in the $SmCo_{1-x}Fe_xO_3$ series led to regular increase of the unit cell parameters in accordance with the Vegard's rule and to the rising deformation of the orthorhombic perovskite structure. In order to study the influence of the cation substitution on the electronic and spin phase transitions in the $SmCo_{1-x}Fe_xO_3$ series the temperature-dependent measurements of structural and transport properties are required. Up to now, *in situ* X-ray synchrotron powder diffraction experiments have been performed for selected $SmCo_{1-x}Fe_xO_3$ specimens. The data evaluation is in progress and the results will be published in a near future.

Acknowledgements. The work was supported in parts by the Ukrainian Ministry of Education and Sciences (Project "Neos") and an ICDD Grant-in-aid program.

References

1. Yu.Liu, J.Ma, J.Li et al., *J.Alloys Compd.*, **488**, 204 (2009).
2. J.Mawdsley, T.Krause, *Appl. Catal.A Gen.*, **334**, 311 (2008).
3. S.Uhlenbruck, F.Tietz, *Mater.Sci.Eng.*, **107**, 277 (2004).
4. C.Michel, E.Delgado, G.Santillan et al., *Mater.Res.Bull.*, **42**, 84 (2007).
5. C.Tealdi, M.Islam, C.Fisher et al., *Solid State Chem.*, **35**, 491 (2007).
6. J.Fergus, *Sens.Actuators*, **123**, 1169 (2007).
7 K.Berggold, M.Kriener, P.Becker et al., *Phys. Rev. B*, **78**, 9 (2008).

8. J.Chang, B.Lin, Y.Hsu et al., *Physica B*, **329**, 826 (2003).
9. C.Chang, B.Lin, H.Ku, *Chinese J. Phys.*, **41**, 41, 662 (2003).
10. M.Itoh, J.Hashimoto, *Physica C*, **341–348**, 2141 (2000).
11. M.Itoh, J.Hashimoto, S.Yamaguchi et al., *Physica B*, **281–282**, 510 (2000).
12. J.Yan, J.Zhou, *J. Goodenough, Phys. Rev. B*, **69**, 69, 134409 (2004).
13. K.Knizek, Z.Jirak, J.Hejtmanek et al., *Eur. Phys. J.*, **47**, 213 (2005).
14. C.Zobel, M.Kriener, D.Bruns et al., *Phys. Rev. B*, **66**, 020402 (2002).
15. Y.Jia, S.Liu, Y.Wu et al., *Phys. Status Solidi A*, **143**, 15 (1994).
16. D.Karpinsky, I.Troyanchuk, K.Barner et al., *J. Phys.:Condens. Matter.*, **17**, 7219 (2005).
17. S.Ivanova, A.Senyshyn, E.Zhecheva et al., *Solid State Chem.*, **183**, 940 (2010).
18. H.Nagamoto, I.Mochida, K.Kagotani et al., *J. Mater. Res.*, **8**, 3158 (1993).
19. Z.Wang, Ch.Chen, C.Feng et al., *Acta Phys.-Chim. Sin.*, **24**, 375 (2008).
20. N.Escalona, S.Fuentealba, G.Pecchi, *Appl. Catal. A_Gen.*, **381**, 253 (2010).
21. O.Kharko, L.Vasylechko, *Visnyk of Lviv Polytechnic National University. Electronics*, **734**, 119 (2012).
22. O.Kharko, L.Vasylechko, Yu.Prots. in: Proc. of 14th European Conference on Solid State Chemistry, Bordeaux, France (2013), p.75.
23. O.Kharko, L Vasylechko, *Visnyk of Lviv Polytechnic National University. Electronics*, **764**, 61 (2013).
24. F.Bartolome, M.Kuz'min, J.Bartolome et al., *J. Magn. Magn. Mater.*, **140–144**, 2159 (1995).
25. R.Zhang, J.Hu, Z.Han et al., *J. Rare Earths*, **28**, 591 (2010).
26. Y.Ren, E.Liu, J.Wang et al., *Rare Metals*, **21**, 190 (2002).
27. Y.Itagaki, M.Mori, Y.Hosoya et al., *Sens. Actuators B*, **122**, 315 (2007).
28. M.Zhao, H.Peng, J.Hu et al., *Sens. Actuator B*, **129**, 953 (2008).
29. O.Kharko, L.Vasylechko, Yu.Prots, in: Proc. of XII International Conference on Crystal Chemistry of Intermetallic Compounds, Lviv, Ukraine (2013), p.144.
30. M.Knapp, V.Joco, C.Bahtz et al., *Nucl. Instrum. Methods A*, **521**, 565 (2004).
31. M.C.Bahtz, H.Ehrenberg, H.Fuess, *J. Synchrotron Radiat.*, **11**, 328 (2004).
32. L.Akselrud, P.Zavalij, Yu.Grin et al., *Mater. Sci. Forum*, **133–136**, 335 (1993).
33. L.Vasylechko, A.Matkovskii, D.Savytskii et al., *J. Alloys Compd.*, **292**, 57 (1999).
34. L.Vasylechko, A.Matkovskii, A.Suchocki et al., *J. Alloys Compd.*, **286**, 213 (1999).
35. S.Sasaki, C.Prewitt, R.Liebermann, *Am. Mineral.*, **68**, 1189 (1983).
36. L.Vasylechko, A.Senyshyn, U.Bismayer, ed. by K.A.Gschneidner, Jr., J.-C.G.Bunzli, V.K.Pecharsky, Handbook on the Physics and Chemistry of Rare Earths, North-Holland, Netherlands (2009), v.39, p.113.